JOURNAL OF SYNCHROTRON RADIATION
ISSN 1600-5775

Structural consequences of transforming growth factor beta-1 activation from near-therapeutic X-ray doses

Timothy Stachowski,[a,b] Thomas D. Grant[a,c] and Edward H. Snell[a,d]*

[a]Hauptman–Woodward Medical Research Institute, 700 Ellicott Street, Buffalo, NY 14203, USA, [b]Cell Stress Biology, Roswell Park Comprehensive Cancer Center, 665 Elm Street, Buffalo, NY 14203, USA, [c]Department of Structural Biology, Jacobs School of Medicine and Biomedical Sciences, State University of New York at Buffalo, 700 Ellicott Street, Buffalo, NY 14203, USA, and [d]Materials Design and Innovation, State University of New York at Buffalo, 700 Ellicott Street, Buffalo, NY 14203, USA. *Correspondence e-mail: esnell@hwi.buffalo.edu

Received 6 February 2019
Accepted 14 April 2019

Edited by E. F. Garman, University of Oxford, England

Keywords: latency-associated peptide; transforming growth factor beta-1; SAXS; radiation damage.

Supporting information: this article has supporting information at journals.iucr.org/s

Dissociation of transforming growth factor beta-1 (TGFβ-1) from the inhibitory protein latency-associated peptide (LAP) can occur from low doses of X-ray irradiation of the LAP–TGFβ-1 complex, resulting in the activation of TGFβ-1, and can have health-related consequences. Using the tools and knowledge developed in the study of radiation damage in the crystallographic setting, small-angle X-ray scattering (SAXS) and complementary techniques suggest an activation process that is initiated but not driven by the initial X-ray exposure. LAP is revealed to be extended when not bound to TGFβ-1 and has a different structural conformation compared to the bound state. These studies pave the way for the structural understanding of systems impacted at therapeutic X-ray doses and show the potential impact of radiation damage studies beyond their original intent.

1. Introduction

X-ray-induced radiation chemistry has been a problem for macromolecular crystallography for decades. Understanding, mitigating and even making use of this unwanted phenomenon has been the theme of many studies (Garman & Weik, 2017). Developments including the accurate assessment of absorbed dose (Paithankar *et al.*, 2009; Brooks-Bartlett *et al.*, 2017), cryocooling (Garman & Owen, 2007) and radical scavenging (Allan *et al.*, 2013), amongst others, have helped to minimize the impact. The doses associated with X-ray crystallographic data collection are large. For example, the recommended upper limit for a crystallographic data set, commonly termed the Garman limit, is 30 MGy (Owen *et al.*, 2006), which is almost four million times the dose that is observed to kill a hamster (Kohn & Kallman, 1957) and 200 billion (10^9) times the dose that an adult receives during an average chest X-ray (ICRP, 2007). The typical regimes of conventional radiotherapy are 0.1–2.0 Gy and >2 Gy (Vaiserman *et al.*, 2018), but treatment regimens using single-fraction doses of 8–30 Gy are not unheard of, which are within the dose range studied here (Timmerman *et al.*, 2010; Gao *et al.*, 2019; Lo *et al.*, 2010). In X-ray crystallographic studies, the initial X-ray dose can damage radiation-sensitive features such as disulfide bonds (Sutton *et al.*, 2013), but it is unknown whether a link can be made between the structural impact of the X-rays used for structural studies and the structural changes that occur at dose levels that are relevant to human health (Barcellos-Hoff *et al.*, 1994). In this study, we use some of the tools developed in the

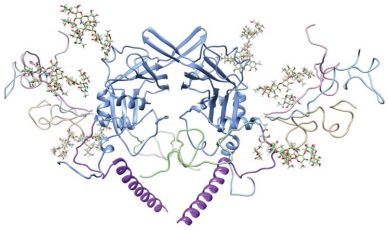

© 2019 International Union of Crystallography

study of X-ray-induced radiation chemistry to probe a biological mechanism that is sensitive to radiation: that of the complex of latency-associated peptide and transforming growth factor beta 1 (TGFβ-1).

TGFβ-1 is a potent cytokine that binds receptors on cell surfaces and initiates signalling pathways that influence numerous processes such as proliferation, wound healing, inflammation, tissue development and tumour cell growth (Bierie & Moses, 2006). Following proteolytic cleavage, the disulfide-linked homodimeric TGFβ-1 is secreted in an inactive form in which it is noncovalently caged by a second disulfide-linked homodimer, latency-associated peptide (LAP), so-called owing to its function of rendering TGFβ-1 latent when in complex. The N-terminal α1 helix and latency-lasso segments in the straightjacket domain of LAP surround TGFβ-1 and maintain the complex, which is called latent TGFβ-1 (LTGFβ-1). Through a process known as activation that is triggered by numerous physiochemical processes such as low pH (Lyons *et al.*, 1988), mechanical stress (Munger *et al.*, 1999; Dong *et al.*, 2017), proteolysis (Sato & Rifkin, 1989) and heat (Lawrence *et al.*, 1985), LAP undergoes a large conformational change that releases TGFβ-1, allowing it to bind receptors and influence cellular phenotypes (Annes *et al.*, 2003; McMahon *et al.*, 1996; Dong *et al.*, 2017; Shi *et al.*, 2011). A schematic illustrating the process is shown in Fig. 1.

LTGFβ-1 also undergoes X-ray radiation-induced activation. Researchers monitoring the changes in protein expression involved in inflammation following exposure to ionizing radiation first observed a rapid induction of TGFβ-1 activity in mammary-gland cells after exposure to 5 Gy (Barcellos-Hoff, 1993). Later work showed that following exposure, an increase in fluorescent staining for activated TGFβ-1 occurred alongside a decrease in staining for LAP (Barcellos-Hoff *et al.*, 1994), suggesting that radiation caused the dissociation of TGFβ-1 from LAP and subsequent activation. This relationship was shown to be dose-dependent (Ehrhart *et al.*, 1997). Interestingly, the irradiation of recombinant protein solutions between 50 and 200 Gy yielded two large populations: activated and inactivatable (*i.e.* damaged) TGFβ-1 (Barcellos-Hoff & Dix, 1996). This suggests two different structural pathways resulting from radiation exposure: activating and damaging. A possible activating pathway is through reactive oxygen species (ROS) that are generated by X-ray radiation. It has been shown that ROS are sensed by a redox centre at a nonconserved methionine in LAP that triggers a conformational change and releases TGFβ-1 (Jobling *et al.*, 2006). Investigations that modulated TGFβ-1 activity using ROS generated from low-powered laser (LPL) irradiation showed a correlated increase of TGFβ-1 activity with free cysteine production following LPL treatment (Arany *et al.*, 2014). While these studies clearly indicate that X-ray doses of up to at least 200 Gy can activate TGFβ-1, the underlying structural mechanism remains unclear. On the other hand, a damaging pathway was hypothesized to occur from the direct photoabsorption of X-rays by the protein (Barcellos-Hoff & Dix, 1996), and the decrease in fluorescent staining for LAP in irradiated tissues was thought to be caused by protein aggregation (Barcellos-Hoff *et al.*, 1994), which is part of the study presented here.

Additionally, disulfide disruption represents an unexplored component of X-ray exposure that is potentially applicable to both the activation and damaging processes. LAP and TGFβ-1 contain disulfides (two and five, respectively) that are known to be essential for proper folding (Brunner *et al.*, 1989; Shi *et al.*, 2011). Disulfides are preferentially sensitive to X-ray radiation because of (i) their higher photoabsorption cross-section relative to other elements in proteins and (ii) desulfurization from solvated electrons generated from the photolysis of water, the consequences of which have been well characterized using crystallographic methods in other proteins (Sutton *et al.*, 2013; Weik *et al.*, 2000; Meents *et al.*, 2010).

LAP sequestration of TGFβ-1 and the numerous modes of activation allow fine spatiotemporal regulation of TGFβ-1 activity. An imbalance in activity, however, leads to numerous pathologies such as Camuarti–Engelmann disease and fibrosis (Drumm *et al.*, 2005; Kinoshita *et al.*, 2000). Additionally, because of the powerful role that it plays in controlling tumour growth, understanding how therapeutic X-ray radiation alters the dynamics of LTGFβ-1 can help to improve therapeutic design (*e.g.* antibody development) or the course of intervention (*e.g.* exposure regimen), ultimately improving treatment outcomes (Gabriely *et al.*, 2017; Wilkinson *et al.*, 2000;

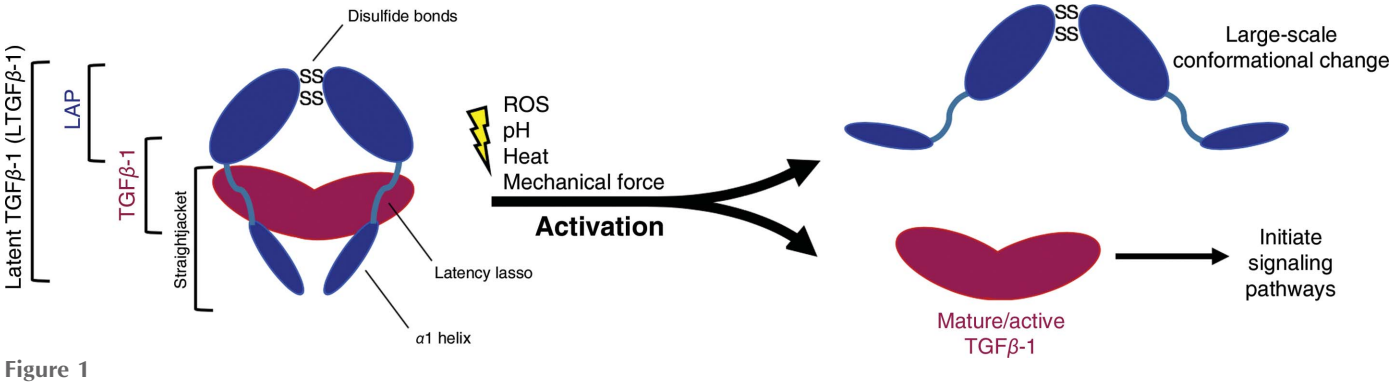

Figure 1
General schematic of LTGFβ-1 activation to show the LTGFβ-1 complex and the activation releasing TGFβ-1. In the latent complex form, the N-terminal α1 helix and latency-lasso segments of the straightjacket domain of LAP cage TGFβ-1, maintain latency and prevent receptor binding (Shi *et al.*, 2011).

Table 1
Construct modifications for protein production of wild-type human LTGFβ-1, ROS-insensitive LTGFβ-1_{M253A}, inactivatable LTGFβ-1_{R249A} and LAP.

Modification	Sequence No.	Application	Sample
N-terminal His tag	30–35	Purification	LTGFβ-1, LTGFβ-1_{M253A}, LTGFβ-1_{R249A}
HRV-3C	36–43	Enzymatic His-tag removal	LTGFβ-1, LTGFβ-1_{M253A}, LTGFβ-1_{R249A}
Methionine→alanine	267 (gene 253)	ROS insensitive	LTGFβ-1_{M253A}
Arginine→alanine	292 (gene 249)	Inhibit proteolytic cleavage	LTGFβ-1_{R249A}
Stop codon	405	Negate original C-terminal His tag	LTGFβ-1, LTGFβ-1_{M253A}, LTGFβ-1_{R249A}, furin
Cysteine→serine	47 (gene 4)	Prevent improper disulfide bonding	LTGFβ-1, LTGFβ-1_{M253A}, LTGFβ-1_{R249A}, LAP

Barcellos-Hoff & Dix, 1996). Additionally, LTGFβ-1 serves as a suitable target for studying the biological impact of radiation damage at a structural level with therapeutic importance.

Here, we investigated the effects of near-therapeutic X-ray radiation exposure on the structure of LTGFβ-1 using small-angle X-ray scattering (SAXS) and complementary techniques to better understand how radiation modulates its biological activity by characterizing the changes induced by radiation exposure, determining the protein regions that are most sensitive to radiation and understanding the radiation chemistry that initiates the process. We report evidence that the previously reported damage pathway manifests as protein aggregation and explore the role of disulfide disruption in X-ray-induced TGFβ-1 activation. Additionally, we show that LAP undergoes a large conformational change when unbound to TGFβ-1.

2. Experimental

2.1. Sample production

Four proteins were used in this study: wild-type human LTGFβ-1, reactive oxygen species (ROS)-insensitive LTGFβ-1_{M253A} (Jobling *et al.*, 2006), inactivatable LTGF-$\beta1_{R249A}$ (Zhao *et al.*, 2018) and LAP. All proteins were produced using the plasmid TGFβ1-bio-his expressing human LTGFβ-1 (Sun *et al.*, 2015). The construct modifications used to produce these proteins are summarized in Table 1. LTGFβ-1_{M253A} lacks a redox-sensing methionine, rendering it ROS insensitive. The LTGFβ-1_{R249A} mutant lacks the proteolytic cleavage site so that TGFβ-1 remains covalently attached to LAP and unable to dissociate. Following the endogenous signal peptide, the original vector was modified by adding a 6×histidine tag for purification followed by a Human rhinovirus 3C protease (HRV-3C) cleavage site through site-directed mutagenesis (Q5 kit, NEB). All constructs include a Cys4-to-serine (C4S) mutation in the LAP domain to prevent improper disulfide bonding and improve expression (Zou & Sun, 2004). A stop codon was inserted after Ser361 to negate the original C-terminal 6×histidine tag. The inactivatable LTGFβ-1_{R249A} control was produced with an Arg249-to-alanine mutation in the $RHRR^{249}$ furin cleavage site. The LAP expression construct was generated by removing the TGFβ-1 domain and was purified using the original C-terminal 6×histidine tag. To produce maximally processed protein, the plasmid furin-bio-his expressing the ectodomain of the human protease furin was obtained, and to prevent co-purification a stop codon replaced the first histidine in the C-terminal purification tag.

The final constructs were expressed in a human endothelial kidney cell (HEK) variant, Expi293-F, that was grown in Expi293 medium and transiently co-transfected with both LTGFβ-1 (98%) and furin (2%) constructs with ExpiFectamine (Thermo Fisher). The cells were cultured for 48–72 h at 37°C with 8% CO_2 before harvesting the medium. The medium was filtered, concentrated tenfold by tangential flow filtration and then diluted tenfold with 10 m*M* Tris–HCl, 0.14 *M* NaCl (TBS) pH 8.0. The protein was purified using Ni–NTA agarose with incubation overnight at 4°C. TGFβ-1 was eluted in the same buffer with the addition of 250 m*M* imidazole. The concentrated protein was further purified and exchanged into 10 m*M* NaH_2PO_4, 1.8 m*M* KH_2PO_4, 2.7 m*M* KCl, 137 m*M* NaCl (PBS) pH 7.4 using a Superdex 200 10/300 size-exclusion column (GE Life Sciences). The protein purity was assessed by SDS–PAGE using 12% acrylamide Mini-PROTEAN Tris–glycine gels (Bio-Rad). All experiments were performed with the fully glycosylated form of LTGFβ-1.

2.2. Sample stability and activity

Protein thermal shift assays (differential scanning fluorimetry; DSF) were conducted to assess protein stability using an Mx3005P real-time PCR system (Agilent); 10 µg protein was placed in 30 µl PBS with 2 µl 75× SYPRO Orange dye (Thermo). The thermal shift of each protein was conducted on a 1% gradient from 25 to 100°C, taking about 40 min. Using a custom *Mathematica* script, the melting temperatures (T_m) were approximated by taking the temperature with the highest value from the first derivative of the fluorescence curve and were averaged across triplicate measurements.

To ensure that the proteins were contaminant-free and monodisperse prior to SAXS experiments, they were characterized using dynamic light scattering (DLS). DLS analyses were carried out using a SpectroLight 600 (XtalConcepts GmbH, Hamburg, Germany). Samples were pipetted onto a 72-well Terasaki plate (Sigma–Aldrich) in volumes of 1 µl of 4 mg ml^{-1} sample. Prior to sample loading, the plates were filled with light paraffin oil (Sigma–Aldrich) to protect the sample solutions from drying out. The laser wavelength used was 660 nm at a power of 100 mW. The scattering angle of the detector was fixed at 150°. The refractive index of water was used for all calculations and measurements were taken at 20°C. The data represent the average of duplicates that were measured 25 times (10 s per measurement).

To confirm that the purified LTGFβ-1 and LAP were biologically active and able to control signalling pathways, activity assays were carried out. Using a phosphospecific

sandwich ELISA, the ability of heat-activated LTGFβ-1 to trigger the phosphorylation of SMAD, a transcription factor in the canonical TGFβ-1 signalling pathway, was measured. TGFβ-1 activity measurements were performed using a PathScan Phospho-Smad2(Ser465/467) sandwich ELISA kit (Cell Signalling Technology) and mouse mammary-gland (NMuMG) cells, which were a gift from Andrei Bakin (RPCCC, Buffalo, New York, USA). Briefly, LTGFβ-1 was thermally activated by incubating the protein in an 80°C water bath for 10 min. Serum-starved NMuMG cells were incubated for 30 min at 37°C with either heat-activated LTGFβ-1 or mature TGFβ-1 (R&D Systems) at the indicated concentrations. The cells were washed twice with ice-cold PBS, harvested and sonicated in the lysis buffer provided by the manufacturer. The cell lysates were applied to wells and the assay was carried out according to the manufacturer's instructions, with the absorbance read at 450 nm using a BioTek Synergy 2 plate reader. Data were averaged across triplicates and fitted to a four-parameter logistic regression (4PL) curve using a custom script in *Mathematica*.

2.3. SAXS data collection

SAXS data were collected for purified LTGFβ-1, LTGFβ-1$_{M253A}$, LTGFβ-1$_{R249A}$ and LAP using the ALS SIBYLS beamline mail-in SAXS service. Four concentrations of each sample were analyzed to determine concentration-dependent effects (2.3, 1.15, 0.58 and 0.29 mg ml^{-1}). Bovine serum albumin (BSA) was used as a control (1 mg ml^{-1}) since its radiation sensitivity has been well characterized (Jeffries *et al.*, 2015) and it is often used as a standard in SAXS experiments (Svergun *et al.*, 2013). Data were collected with all proteins in PBS. To probe the mechanism of damage, scavengers (Allan *et al.*, 2013) were separately added in the form of ascorbic acid (a ROS scavenger) and sodium nitrate (an electron scavenger) to 1 mg ml^{-1} protein solutions at 10 m*M* concentration and 2%(*v*/*v*) glycerol (a ROS scavenger that also inhibits aggregation) using all four conditions for LTGFβ-1, LTGFβ-1$_{R249A}$ and LAP, and just the first two conditions for all four samples, as LTGFβ-1$_{M253A}$ was not available in a sufficent volume. SAXS data were then collected in a similar manner. The protein concentrations used for data collection were determined from the absorbance at 280 nm. The photon energy used throughout was 11.0 keV (1.13 Å). Momentum-transfer values were calculated as $q = 4\pi \sin\theta/\lambda$, where 2θ is the scattering angle and λ is the X-ray wavelength in Å. Data were recorded using a PILATUS 2M detector from Dectris. Error bars were estimated using the *GNOM* program from *ATSAS* (Franke *et al.*, 2017). A volume of 25 µl of each sample was loaded into the sample chamber. The exposure time for each frame was 0.1 s and a total of 50 frames were collected for each sample with the sample kept static. Buffer from the SEC flowthrough was used for matched controls and buffer subtraction. The buffers used for subtraction for the samples irradiated in the presence of scavengers also contained the matching scavenger. The beamline staff evaluated the flux at the sample to be 1.2 × 10^{12} photons s^{-1}. *RADDOSE-3D* modified for SAXS experiments (Brooks-Bartlett *et al.*, 2017) was used to calculate the dose rate (142 Gy s^{-1}), taking into account the attenuation by the sample container, the beam type and the beam dimensions. The parameters used for this calculation are available in Supplementary Table S2. The dose of each 0.1 s frame collected was 14.2 Gy. Details of the data collection and processing are provided in Supplementary Table S1 following standard guidelines (Trewhella *et al.*, 2017).

2.4. SAXS data analysis

For further analysis of the LTGFβ-1 and LAP solution structures, data from multiple exposures were averaged to increase the signal to noise. The *ATSAS* program suite (EMBL) was used for all data analysis (Franke *et al.*, 2017), except where noted otherwise. For LTGFβ-1, 49 exposures from the 1 mg ml^{-1} 2% glycerol sample were averaged using *PRIMUS* as they exhibited no radiation damage upon analysis of R_g, $I(0)$ and the total scattering profile shape using *CorMap* (Franke *et al.*, 2015). For LAP, the first four exposures from the 4.5 mg ml^{-1} sample were averaged as they exhibited no radiation damage using the same analysis. The R_g values reported were calculated from the Guinier region with ranges according to $q_{max} \times R_g = \sim 1.3$. The theoretical R_g values of 3D models that were used for comparison with the experimental values were calculated using *CRYSOL*. *MODELLER* was used to build missing loops into models (Webb & Sali, 2014). Total integrated intensities were calculated according to the composite trapezoidal rule using a custom Python script with the NumPy module. To monitor the change in intensity over time, total integrated intensities at each dose, I_D, were normalized to the total integrated intensity at the first dose point, $I_{14.2}$. The total integrated intensity, although yielding no obvious structural insight, is sensitive to any change in the scattering profile (Hopkins & Thorne, 2016) and is particularly sensitive with short exposures (Semisotnov *et al.*, 1996) or the low doses used in this case.

2.5. Conformational heterogeneity

The conformational heterogeneity of LAP was assessed with the *Ensemble Optimization Method* (*EOM*), which generates an ensemble of structures with alternative conformations that best explain the experimental SAXS data (Tria *et al.*, 2015). Using the LAP dimer from the LTGFβ-1 crystal structure, the straightjacket domain (α1 helix and latency lasso; amino acids 1–45) was removed (Shi *et al.*, 2011). The program *RANCH* (part of *EOM*) was used with *P*2 symmetry to generate 30 000 independent models in which the straightjacket domain was rebuilt in random conformations. The program *GLYCOSYLATION*, which is part of *ATSAS* (Franke *et al.*, 2017), was used to add six N-glycans according to molecular mass, position and branch type as determined biochemically (Barnes *et al.*, 2012). Structures in which the random orientation of the modelled region sterically clashed with the placement of the N-glycan as indicated by *GLYCOSYLATION* were omitted, leaving a final pool of

10 000 models. The theoretical scattering of the resulting pool was calculated using *CRYSOL*. Afterwards, a genetic algorithm (the *GAJOE* program, also part of *EOM*) was used to select an ensemble of conformations from the random pool that best explained the experimental SAXS data and this was repeated 100 times, with the ensemble with the lowest discrepancy reported.

2.6. CD spectroscopy

To provide information on secondary structure, CD spectroscopy was used. Purified LTGFβ-1 and LAP were exchanged into 10 m*M* phosphate buffer pH 7.4, 150 m*M* sodium fluoride using a Zebo desalting column (Thermo Fisher) and diluted to 2.5 µ*M*. Far-UV CD spectra were measured using a JASCO-815 spectrophotometer. All measurements were made at 25°C in a 0.1 cm path-length cell. The spectral bandwidth was held constant at 1.0 nm. Spectra were recorded from 250 to 190 nm. Three replicates of each measurement were made and are presented as the mean residue ellipticity (deg cm^2 dmol^{-1}). The theoretical CD spectra for the LTGFβ-1 crystal structure (PDB entry 3rjr; Shi *et al.*, 2011) were calculated using the *PDB2CD* webserver (Mavridis & Janes, 2017). Approximation of the secondary-structure content of the experimental spectra was carried out using the *BeStSel* webserver (Micsonai *et al.*, 2018).

3. Results

Analysis of the purified protein by SDS–PAGE showed the LTGFβ-1 to be highly pure and showed that under nonreducing conditions it migrates as two bands to molecular weights corresponding to the glycosylated LAP dimer (75 kDa) and TGFβ-1 dimer (25 kDa). Under reducing conditions, both LAP and TGFβ-1 migrate to molecular weights that match those of their respective monomers: 37.5 and 12.5 kDa, respectively (Supplementary Fig. S1).

The DSF analysis showed that all of the proteins produced exhibited typical sigmoidal fluorescence curves, indicating well folded protein. As expected, LTGFβ-1, LAP and LTGFβ-1$_{M253A}$ exhibited melting temperatures of 70–75°C, which are near the established temperature of 75°C that is necessary for complete thermal activation of LTGFβ-1. This indicates that LAP, even without TGFβ-1 bound, remains largely folded, as also observed using atomic force microscopy experiments (Buscemi *et al.*, 2011). The inactivatable mutant LTGFβ-1$_{R249A}$ exhibited a higher melting temperature of 82°C, which is presumably owing to LAP being covalently bound to TGFβ-1, stabilizing the complex (Supplementary Fig. S2). SEC and DLS measurements showed a uniform distribution, indicating a monodisperse and contaminant-free sample (Supplementary Fig. S3).

Following the incubation of mouse mammary-gland (NMuMG) cells with increasing concentrations of heat-activated LTGFβ-1, an EC$_{50}$ value of 23.2 p*M* was measured. This was lower than the activity of mature commercially available TGFβ-1 (3.46 p*M*; R&D Systems; Fig. 2). This discrepancy was unsurprising considering the ability of LAP to rebind and inhibit activity and the loss of some mature TGFβ-1 owing to denaturation during heat treatment. Similarly, titrating LAP against a fixed amount of TGFβ-1 (10 p*M*) showed a dose-dependent decrease in signal, with an IC$_{50}$ value of 5.7 p*M* and with complete signal quenching at a 1:1 stoichiometry (Fig. 2). Together, these results show that the recombinant proteins are biologically active and therefore structurally sound.

SAXS is a particularly useful technique for studying X-ray radiation-induced TGFβ-1 activation as the process can be simultaneously initiated and monitored for structural changes. Radiation damage to proteins in SAXS results in fragmentation, aggregation and unfolding, all of which can be monitored by changes in the scattered intensity (Hopkins & Thorne, 2016). An increase in intensity indicates damage leading to protein aggregation, while a decrease in intensity suggests dissociation of LAP from TGFβ-1 (*i.e.* activation). In this case,

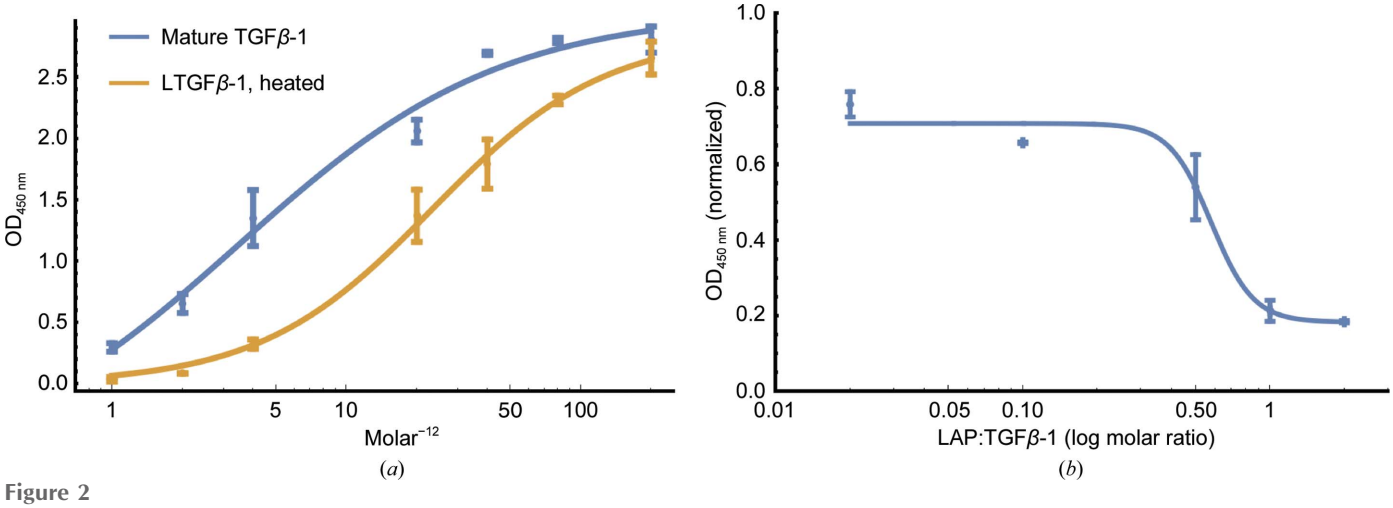

Figure 2
Titrations of in-house recombinant proteins trigger canonical TGFβ-1 signalling pathways at the expected levels. (*a*) Levels of SMAD phosphorylation for commercial mature TGFβ-1 (blue) and in-house heated LTGFβ-1 (gold). (*b*) Titration of LAP against a fixed amount of mature TGFβ-1 (10 p*M*). Data were fitted to a four-parameter logistic regression (4PL) to determine the EC$_{50}$ and IC$_{50}$ values. (*a*) The EC$_{50}$ values were 23.2 and 3.46 p*M* for in-house heated LTGFβ-1 and commercial TGFβ-1, respectively. (*b*) The IC$_{50}$ for LAP was 5.7 p*M* (0.57 molar ratio).

four concentrations of each sample were irradiated using a low-dose data-collection strategy at 142 Gy s^{-1} for 49 exposures captured at 0.1 s per exposure (14.2 Gy diffraction-weighted dose) with a maximum accumulated dose of 696 Gy. For comparison, most SAXS experiments deliver doses in the 1–10 kGy range (Hopkins & Thorne, 2016). At the higher concentrations irradiated (2.3 and 1.15 mg ml^{-1}), LTGFβ-1 exhibited a dose-dependent increase in the intensity at low q and a departure from linearity in the Guinier plot, which are indicative of aggregation [Fig. 3(*a*)]. To compare between samples and across doses, the change in the total scattered intensity at each dose point (I_D) was integrated and normalized to the total intensity after the first dose ($I_{14.2}$). Since the presence of larger species (aggregates) has a larger impact on the total scattering than an equal amount of smaller species (in this case dissociation products), it is possible that the generation of aggregates might overshadow decreases in the intensity from TGFβ-1 dissociation. However, no change in the total integrated intensity was observed at low concentrations (0.58 and 0.29 mg ml^{-1}) even after the maximum accumulated dose [Fig. 3(*b*)]. This suggests that X-ray radiation alone is not sufficient for the dissociation of TGFβ-1 from LAP, and correspondingly TGFβ-1 activation, and that small-scale structural changes that perhaps prime LTGFβ-1 for activation may be required. Radiation may therefore influence TGFβ-1 through two pathways: (i) the prevention of subsequent activation owing to damage leading to aggregation and (ii) small-scale structural changes that perhaps prime LTGFβ-1 for dissociation and activation. This may explain the previous findings that irradiation of LTGFβ-1 results in two populations of activated and damaged (*i.e.* aggregated) protein (Barcellos-Hoff & Dix, 1996).

There was also a marked difference in the propensity for aggregation of the different TGFβ-1 proteins tested. Compared with LTGFβ-1 at the same concentration (1 mg ml^{-1}), LAP exhibited a greater increase in intensity after the maximum accumulated dose of 696 Gy, with an $I_{696}/I_{14.2}$ of 1.25 and 1.35, respectively. This suggests that it is more sensitive to radiation when unbound to TGFβ-1 than when complexed with TGFβ-1 in the latent form [Fig. 4(*a*)]. The two mutants expected to limit dissociation, LTGFβ-1_{M253A} and LTGFβ-1_{R249A} ($I_{696}/I_{14.2}$ of 1.10 for both), also showed a marked decrease in aggregation compared with both LTGFβ-1 (1.25) and LAP (1.35) after 696 Gy [Fig. 4(*b*)]. Compared with the TGFβ-1 proteins, when irradiated in PBS alone BSA did not show a strong relationship between dose and intensity, and only showed an increase in intensity when approaching the maximum dose. While no expected dissociation in any protein was detected, as shown by a constant total integrated intensity, these results show that LAP is more sensitive to radiation-induced aggregation when unbound to TGFβ-1. Flexibility and conformation analysis, given below, show that there is a large conformational difference in LAP when unbound to TGFβ-1 and when bound (*i.e.* latent). This difference might contribute the increased sensitivity to radiation-driven aggregation. Similarly, since the inactivatable mutants showed reduced aggregation compared with wild-type LTGFβ-1 in all conditions, this also suggests that aggregation includes some type of unfolding in the wild type that is prohibited in the inactivatable mutants. On the other hand, protein aggregation is typically thought of as a nonspecific process driven by charge buildup on the surface of the protein molecules, which then become cross-linked with each other during diffusive collisions (Kuwamoto *et al.*, 2004). For the inactivatable LAP mutants, the residues Met253 and Arg249 are on the surface. Reducing the surface charge with alanine mutations in these residues might have resulted in reduced aggregation.

ROS can trigger TGFβ-1 activation through the redox-sensing Met253 (Barcellos-Hoff *et al.*, 1994). Additionally, LTGFβ-1 contains numerous disulfides that are targets for disruption by solvated electrons, which are also generated by X-ray radiation, but this possible pathway has never been explored. To study this, scavengers with different properties were explored. When irradiated in the presence of 10 m*M* ascorbic acid (a ROS scavenger), all constructs showed no dose-dependent change in intensity [Fig. 4(*b*)]. A similar

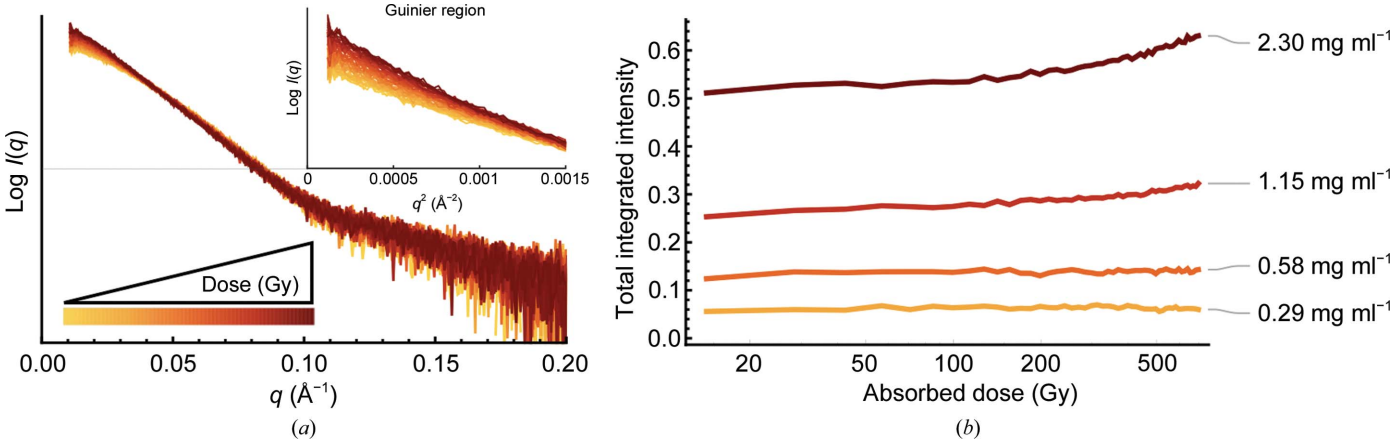

Figure 3
Scattered intensity from the SAXS signal increases as a function of radiation dose and concentration. (*a*) Scattering profiles of LTGFβ-1 (2.3 mg ml^{-1}) show an increase in intensity at low q as a function of dose (inset), indicating aggregation. (*b*) LTGFβ-1 was irradiated at four concentrations, exhibiting a dose-dependent increase in the total integrated intensity at higher concentrations that suggests aggregation, but no change in intensity at low concentrations.

response was seen in the presence of 2% glycerol, which has a similar mechanism to ascorbic acid while also stabilizing protein surfaces [Fig. 4(*c*)]. Irradiation of proteins in 10 m*M* sodium nitrate (a solvated electron scavenger) exhibited a moderate dose-dependent increase in aggregation [$I_{696}/I_{14.2}$ of 1.1–1.2; Fig. 4(*d*)], but this response was greatly reduced compared with proteins irradiated in PBS alone [$I_{696}/I_{14.2}$ of 1.1–1.35; Fig. 4(*a*)]. In comparison, bovine serum albumin (BSA) showed no preference between scavengers, showing that the observed preferential sensitivity of LTGFβ-1 to ROS-induced aggregation is not a necessary component of radiation-induced aggregation in proteins. Previous studies showed that TGFβ-1 was activated by the hydroxyl radical (Jobling *et al.*, 2006). These results show that ROS are generated during irradiation and that they are also the primary source of aggregation. It should be noted that irreversible aggregates can be generated during sample preparation and concentration, which can then be carried into diluted samples. The presence of these aggregates can then promote the formation of further aggregates through cooperation (Winklmair, 1971). However, the presence of aggregates in our samples prior to irradiation was ruled out by SEC and DLS experiments at higher concentrations (4 mg ml^{-1}) [Supplementary Figs. S3(*a*) and S3(*b*)]. Because no decrease in intensity was observed in the presence of any scavenger, and because the inactivatable mutants showed a decreased propensity for aggregation, the results are not inconsistent with a pathway in which X-ray radiation could cause a small-scale structural change, priming LTGFβ-1 for activation.

Although the crystal structure of LTGFβ-1 has been solved (Shi *et al.*, 2011), the structure of unbound LAP has not. The conformation of LAP when unbound to TGFβ-1, which is a key state during cellular LTGFβ-1 complex processing and following activation in the extracellular matrix, has not been determined. Initial fitting of the LTGFβ-1 experimental curve to the crystal structure (PDB entry 3rjr) was poor [χ^2 = 95.0; Fig. 5(*a*)]. The fit improved (χ^2 = 3.56) by glycosylating the model according to the approximate molecular weight and

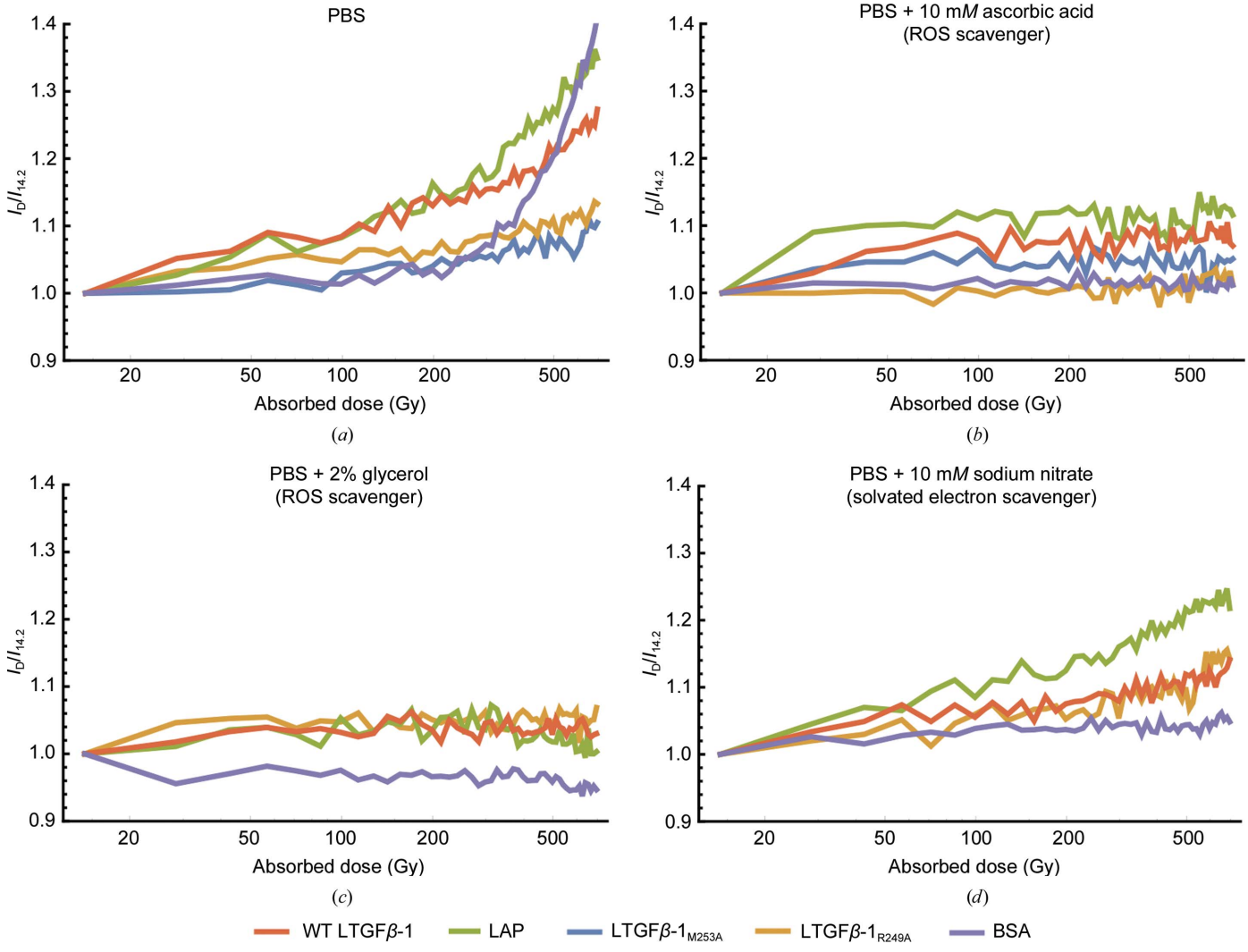

Figure 4
Comparison of dose-dependent changes in the total integrated intensity (I) with protein at 1 mg ml^{-1} irradiated in solution with different radical scavengers shows that ROS is the predominant cause of aggregation. (*a*) Protein irradiated in PBS alone, (*b*) in PBS and 10 m*M* ascorbic acid, (*c*) in PBS and 2% glycerol and (*d*) in PBS with 10 m*M* sodium nitrate.

branch type of the sample as determined biochemically (Barnes *et al.*, 2012). However, this same glycosylation treatment (χ^2 = 17.41) applied to the model of the LAP domain alone (χ^2 =147.35) did not provide a convincing fit to the LAP experimental data [Fig. 5(*b*)].

LAP binds TGFβ-1 in the latent form by caging it with the straightjacket domain. This domain contains the α1 helix and is connected to LAP by a flexible linker: the latency lasso (Fig. 1). This arrangement suggests that this helix of LAP should be flexible when TGFβ-1 is unbound. From the Guinier analysis of data from the unaggregated sample, LAP has a larger radius of gyration (R_g) than LTGFβ-1, 40.71 $\pm$ 0.09 and 38.3 $\pm$ 0.59, respectively, which suggests that LAP has a more extended conformation when unbound to TGFβ-1 (Supplementary Table S1). The observation that LAP is extended when unbound to TGFβ-1 is complemented by comparisons of the LAP and LTGFβ-1 scattering curves with a Kratky plot [Fig. 6(*a*)]. While LTGFβ-1 yields a bell-shaped intensity decay typical of a well folded globular particle, LAP exhibits a more gradual intensity decay with a plateau that indicates that it is partially flexible [Fig. 6(*a*)]. The *Ensemble Optimization Method* (*EOM*; Tria *et al.*, 2015; Bernadó *et al.*, 2007) was used to search for an ensemble of glycosylated models with different conformations of the helix and latency lasso that best explain the LAP scattering data. A visual inspection of the curves indicates that the fit to the experimental data was improved and this is also evident from the reduced χ^2 value for the glycosylated model treated as a flexible ensemble (χ^2 = 6.71) versus the rigid glycosylated model (χ^2 = 17.41). *EOM* analysis revealed a bimodal distribution of states in which LAP exists as a mixture of compact (22%) and mostly extended (78%) conformations (Fig. 6, Table 2). LAP can both bind and release TGFβ-1 (Fig. 2). These results indicate, however, that the rebinding of TGFβ-1 to LAP is most likely to be occluded when LAP is in a compact conformation. Although the fit of the final *EOM* ensemble to the experimental LAP data markedly improved the χ^2 value, it is imperfect, especially at low *q*. This can be explained owing to the modelling of the glycosylation as homogeneous, whereas it is more likely to exist as a polydisperse mixture of particles with varying degrees of glycosylation.

Table 2
Secondary-structure comparison between experimental LAP and LTGFβ-1 CD spectra and crystal structures.

Values for $LAP_{\Delta\alpha1\ helix}$ were calculated by treating the α1 helix as disordered.

Sample	LTGFβ-1 (PDB entry 3rjr)†	LAP (PDB entry 3rjr, LAP domain)†	$LAP_{\Delta\alpha1\ helix}$ (PDB entry 3rjr, LAP domain)†	LTGFβ-1	LAP
Helix (%)	19	23.5	12.8	16.6	5.5
Sheet (%)	31	27.5	27.6	34.1	22.8
Turn (%)	8.5	7.6	NA	12.6	17.4
Other (%)	NA	NA	NA	36.7	54.3

† Taken from *DSSP* assignment to crystal structure.

The SAXS analysis, which indicates that LAP is likely to adopt a more extended and unstructured conformation when unbound to TGFβ-1, is supported by the CD spectroscopy data. These show that LAP is less structured when unbound to TGFβ-1 than when bound. The far-UV experimental CD spectra of LAP and LTGFβ-1 and the theoretical CD spectra calculated from the LTGFβ-1 crystal structure (PDB entry 3rjr) using *PDB2CD* revealed that while the experimental

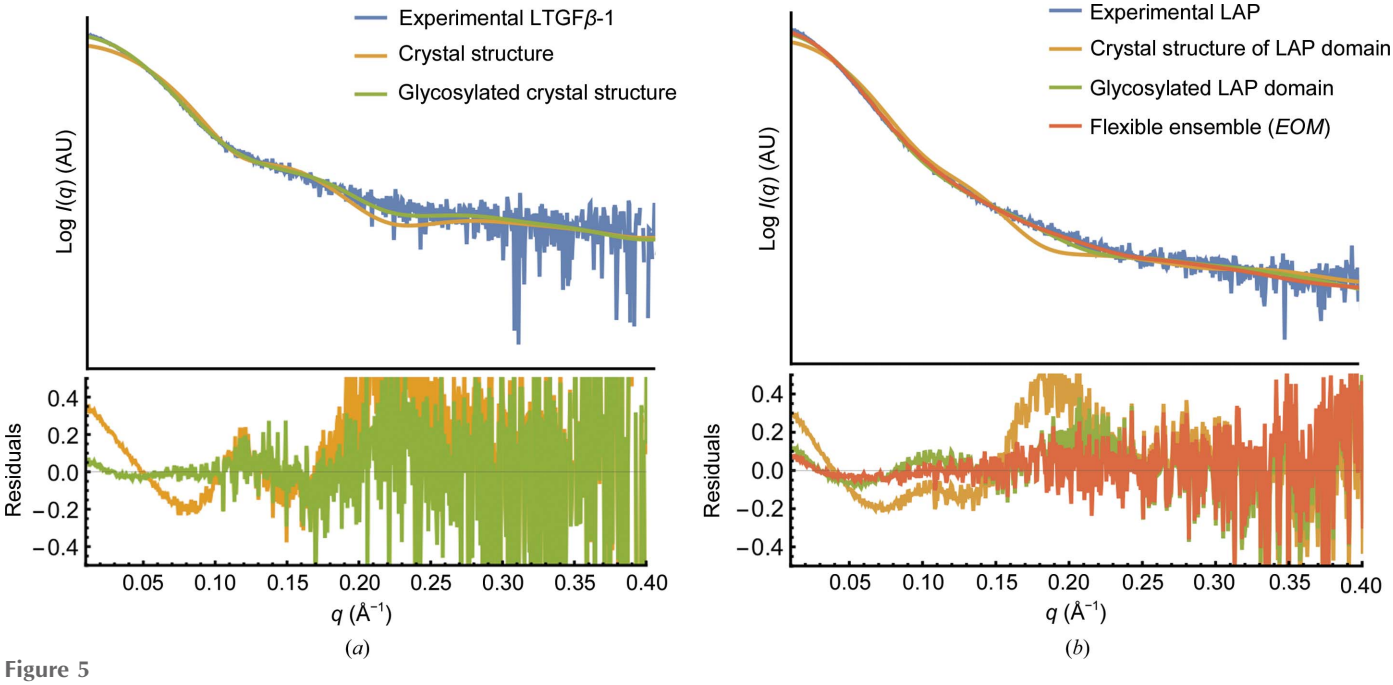

Figure 5
Modelling glycosylation and conformational heterogeneity explains the SAXS data better than comparison with the crystal structure alone. (*a*) Comparison of the experimental LTGFβ-1 scattering profile (blue) with that of a monomer from the crystal structure (PDB entry 3rjr, orange; χ^2 = 95.0) and the glycosylated model (green; χ^2 = 3.56). (*b*) Comparison of the experimental LAP scattering profile (blue) with that of the LAP domain from the LTGFβ-1 crystal structure (orange; χ^2 = 147.35), the glycosylated model (green; χ^2 = 17.41) and the *EOM* ensemble (red; χ^2 = 6.71).

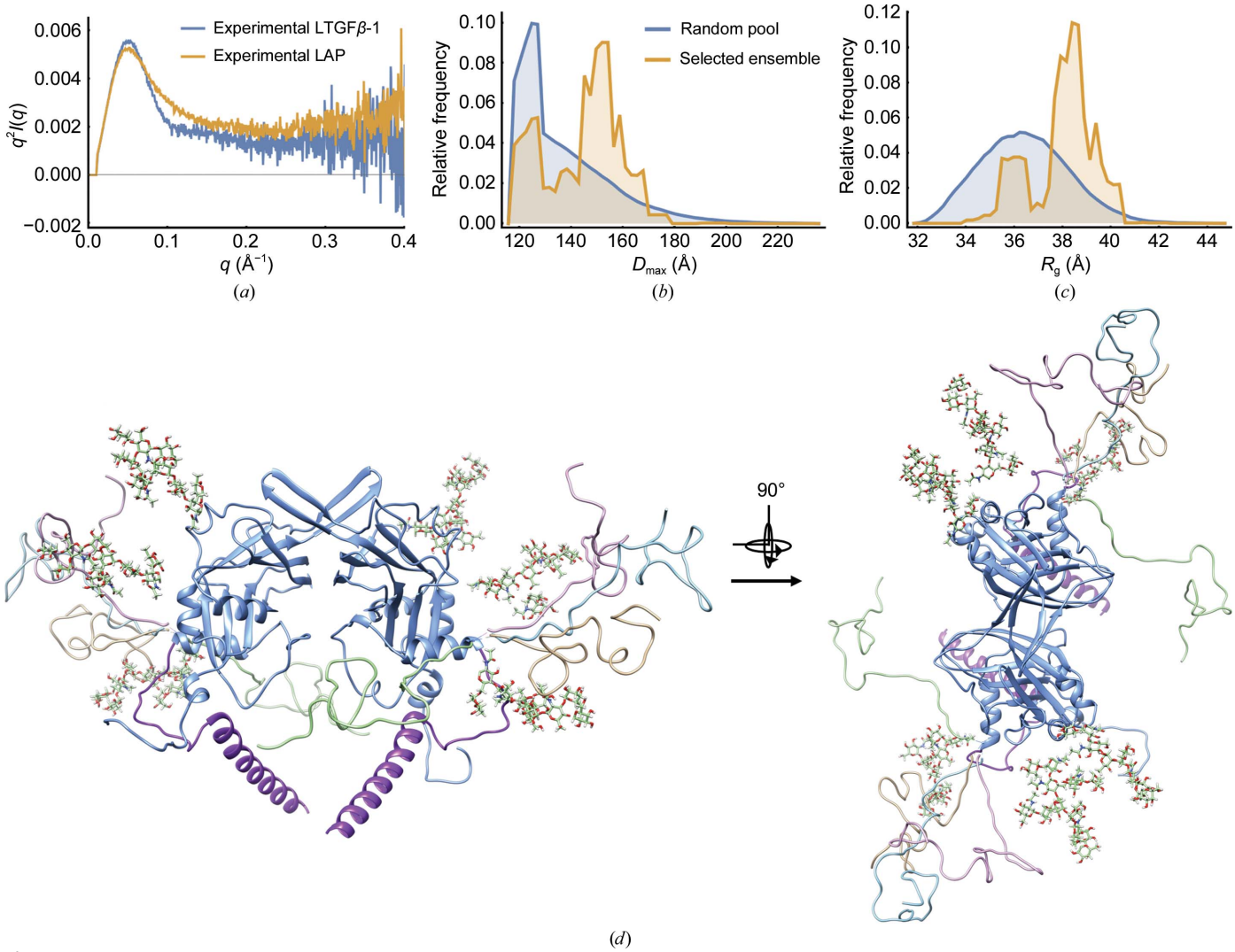

Figure 6
Modelling of SAXS to an ensemble of conformations reveals that LAP exists predominantly in an extended conformation. (*a*) A Kratky plot comparing experimental SAXS profiles for LTGFβ-1 and LAP shows that LAP is more flexible. (*b*) The maximum particle dimension (D_{max}) of the *EOM* random pool (blue) and of the ensemble that best explains the LAP scattering data (gold). (*c*) The radius of gyration (R_g) of the *EOM* random pool (blue) and of the ensemble (gold). (*d*) The LAP domain from the LTGFβ-1 crystal structure (blue; latency helix, purple; glycosylation, various) superimposed with models from the selected ensemble (gold, light blue, green, light purple).

spectrum of LTGFβ-1 agrees well with the theoretical spectrum calculated from the crystal structure, LAP exhibits a deviation compared with the theoretical spectrum of the crystal structure with the TGFβ-1 domain subtracted [Fig. 7(*a*)]. This suggests that LAP undergoes a secondary-structural change when binding/unbinding TGFβ-1. Using *BeStSel* (Micsonai *et al.*, 2018), LAP is estimated to contain 5.5% helix compared with 23.5% when bound to TGFβ-1 (Table 2). This estimated helical content of LAP agrees well with the secondary structure from the crystal structure if the large N-terminal α1 helix of the straightjacket domain that cages TGFβ-1 is treated as unstructured, which yields 13% helix. Together with the extended conformations produced in *EOM*, the data suggest that the binding of TGFβ-1 stabilizes the unstructured straightjacket domain, allowing the formation of the large α1 helix that cages TGFβ-1. *EOM* and CD both indicate a difference in the structure of LAP when unbound versus that when bound to TGFβ-1, implying a large-scale structural change in LAP upon TGFβ-1 binding and unbinding (activation). Since this process was not observed during X-ray radiation exposure, X-ray radiation is not sufficient for activation within the time frame observed, but may serve to prime LAP for TGFβ-1 dissociation through other small-scale structural changes.

4. Discussion and conclusion

Tools developed to mitigate and understand radiation chemistry in crystallographic studies were used to probe the X-ray-induced modulation of LTGFβ-1 activity, a process that has important therapeutic implications. Activation and the prevention of activation (*i.e.* damage) are known to occur at X-ray doses between 100 mGy and at least 200 Gy (Barcellos-Hoff *et al.*, 1994). While the study described here was unable to

probe doses lower than 14.2 Gy, it is still in the regime of therapeutic interest. In comparison, a single crystallographic image is recorded with doses of the order of kilograys and a complete data set with doses measured in megagrays. To understand the biologically important activation process, scavengers with different scavenging mechanisms developed in the study of radiation damage were utilized. Biologically active and stable protein was irradiated in the solution state.

The SAXS studies on continuous irradiation of LTGFβ-1 at higher concentrations yielded a dose-dependent increase in aggregation. LTGFβ-1 is ROS sensitive, and the activation pathway is mediated through Met253 in LAP (Jobling *et al.*, 2006). When LTGFβ-1 was irradiated in the presence of different radical quenchers, the results showed that the aggregation observed was more impacted by oxidative stress. The role of X-ray-generated reductive stress has previously been unexplored. The quenching of solvated electrons yielded a reduced but not completely abolished propensity for aggregation in both wild-type LTGFβ-1 and LAP, which suggests that disulfide-bond disruption is involved in X-ray radiation sensitivity. Together, these results indicate that the TGFβ-1 damage pathway that renders LTGFβ-1 inactivatable and was noted by Barcellos-Hoff & Dix (1996) is predominantly initiated by a similar mechanism to the activation pathway, *i.e.* X-ray radiation-generated oxidative stress, but in combination with a less influential reductive-stress component that leads to protein aggregation. While the concentrations studied here are much higher than those *in vivo*, oxidative stress-induced protein aggregation in the crowded cellular environment has been well documented (Squier, 2001; Grune *et al.*, 1997; Cecarini *et al.*, 2007).

The biochemical and biophysical experiments (DSF and DLS) reported here (Supplementary Figs. S2 and S3) and by others (Buscemi *et al.*, 2011) show that the overall structures of LAP bound to TGFβ-1 and of unbound LAP are almost indistinguishable with certain methods. However, the narrow R_g distribution from *EOM* analysis with SAXS reveals that the straightjacket domain in LAP is likely to be extended and is sampling both compact and extended conformations when TGFβ-1 is unbound [Fig. 6(*c*)]. The CD results reported previously (McMahon *et al.*, 1996), together with those reported here, support the indication from SAXS that there is a notable structural change: LAP unbound to TGFβ-1 has a smaller helical content (5.5%) than when bound (23.5%). This decrease in helical content indicates that the α1 helix within the straightjacket domain that normally cages TGFβ-1 is unstructured when TGFβ-1 is unbound. This large difference between the two binding states of LAP suggests that the release of TGFβ-1 includes a large structural change in LAP and is consistent with investigations of the mechanical unfolding activation pathway.

The role of the α1 helix in the straightjacket domain of LAP in X-ray-induced TGFβ-1 activation is indicated by the results when comparing the radiation sensitivity between LAP, TGFβ-1 and mutants (Fig. 4). Continuous irradiation of samples showed that LAP was more sensitive to radiation-induced aggregation than LTGFβ-1 (LAP bound to TGFβ-1). Similarly, two mutations in LAP that were expected to limit TGFβ-1 dissociation, LTGFβ-1$_{M253A}$ (ROS insensitive) and LTGFβ-1$_{R249A}$ (covalently linked LTGFβ-1), were notably less prone to aggregation. One reason for the increased susceptibility of LAP to radiation-induced aggregation compared with LTGFβ-1 may be the extended and unstructured straightjacket α1 helix of unbound LAP identified by CD and *EOM* (Figs. 6 and 7). This region is most likely to be less stable and more vulnerable to oxidative attacks and, because of its extended conformation, is more likely to become cross-linked to other molecules. Since the two inactivatable mutants tested here both showed a greatly reduced propensity for aggregation, this helical to unstructured and

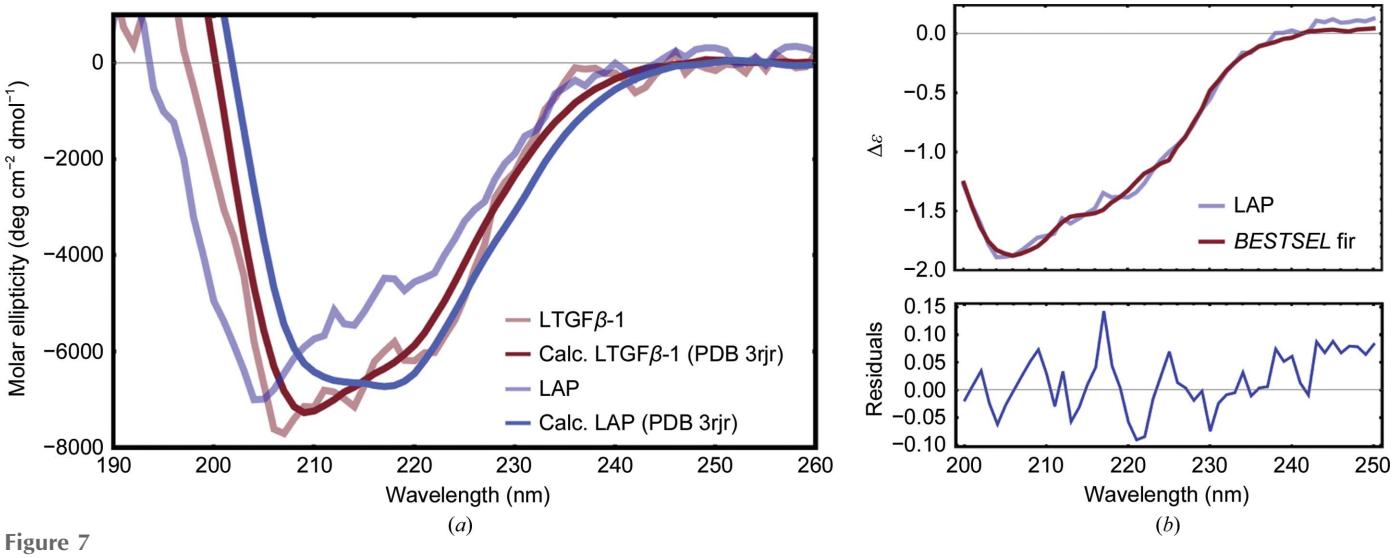

Figure 7
Circular-dichroism spectra show that the secondary structure of LAP is different when unbound and bound to TGFβ-1 (LTGFβ-1). (*a*) Experimental spectra of LTGFβ-1 (light red) and LAP (light blue) compared with theoretical spectra of the crystal structure (LTGFβ-1, dark blue; LAP domain, dark red) calculated with *PDB2CD*. (*b*) Top, representative fit using *BeStSel* of the secondary-structure population approximation (red) of experimental LAP (blue); bottom, the residuals.

extended transition (which is prohibited in the inactivatable mutants) might also be occurring in wild-type irradiated LTGFβ-1, leading to aggregation. Another possible reason for the reduced sensitivity of the mutants is from a reduction in the surface charge. For most proteins, aggregation is typically thought of as a nonspecific process driven by charge buildup on the surfaces of the protein, which then become cross-linked during diffusive collisions (Kuwamoto *et al.*, 2004). These results might indicate a site-specificity of charge buildup, because Met253 and Arg249 are on the surface of LAP and reducing the surface charge with alanine mutations resulted in reduced aggregation.

However, at low concentrations no change in the overall intensity during irradiation of LTGFβ-1 was observed. There was no evidence of either aggregation or the expected radiation-induced dissociation of TGFβ-1 from LAP (activation). One possibility is that competing processes of aggregation and generation of smaller species (dissociation of TGFβ-1 from LAP) may become convoluted when examining the total scattered intensity. The signal at these lower concentrations, however, is too low to fully analyse the scattering-profile shape to assess this possibility. Another explanation is that the dissociation of TGFβ-1 from LAP is triggered by a relatively subtle conformational change. This may not be sufficient to completely drive TGFβ-1 dissociation from LAP in the time frames studied. Small structural priming from X-ray exposure might explain the discrepancy between the results presented here and those in the studies by Barcellos-Hoff & Dix (1996), which investigated X-ray-induced activation by irradiating the protein and measuring biological activity through cellular assays. In this way, the dissociation of TGFβ-1 from LAP is initiated by X-rays but might be completed by a second process that occurs in cells, such as proteolysis or mechanical unfolding (Dong *et al.*, 2017; Annes *et al.*, 2003).

Why this structural transition leads to aggregation and not to the expected dissociation was not answered in this study, despite the evidence that it occurs. However, understanding X-ray-induced aggregation as a structural pathway that damages LTGFβ-1 and prevents activation is an important consideration for modulating TGFβ-1 activity, an area of great therapeutic interest (Gabriely *et al.*, 2017; Wilkinson *et al.*, 2000). It is possible that dissociation was not observed owing to the high dose rate (142 Gy s^{-1}) used in these experiments compared with that used in previous studies (5.3 mGy s^{-1}; Barcellos-Hoff *et al.*, 1994; Ehrhart *et al.*, 1997). Successive doses at the high rate in the study here might damage molecules in a way that prevents dissociation more quickly than an unfolding process can occur. Specifically, oxidation-induced cross-linking that manifests as aggregation might similarly cross-link TGFβ-1 to LAP, preventing dissociation of the LTGFβ-1 complex. This is further supported by the comparison of X-ray sensitivity, in which the decreased aggregation observed in the inactivatable mutants compared with wild-type LTGFβ-1 suggests that X-ray-induced unfolding is occurring, most likely in the straightjacket domain, that would normally allow the release of TGFβ-1.

Additionally, the X-ray energy and source used for these experiments may have an impact. Barcellos-Hoff *et al.* (1994), and Ehrhart *et al.* (1997) used 1.3 MeV ^{60}Co γ radiation. This affects aqueous solutions in the same manner as X-ray radiation (Hochanadel, 1952), but dose-rate effects may play an unknown role. While an understanding of X-ray-induced activation is far from complete, the results here illuminate components of the process, namely that the deactivation mechanism is through oxidation-induced aggregation and that the binding/unbinding of TGFβ-1 by LAP includes a helical-to-disordered transition in the straightjacket domain. Also, we observed a large difference in the X-ray radiation sensitivity between wild-type LTGFβ-1 and the ROS-insensitive mutant, LTGFβ-1_{M253A}, which was first identified as a redox sensor by Jobling *et al.* (2006). This agrees with that study, suggesting that a trigger for this process is located away from the site of the structural change in LAP (*i.e.* the straightjacket domain). No crystallographic structure of LAP is available as the potential glycosylation and presumed disordered regions present structural challenges.

Beyond the focus on TGFβ-1 dissociation in LTGFβ-1, this study has a broader impact. Structural biology using X-ray crystallographic techniques remains the predominant method to understand biological structure and ligand binding. As X-ray sources have advanced, the increased flux density and therefore dose have allowed increasing detail and opened up more systems to structural study. This detail has been at the expense of introducing radiation-chemistry effects that impact the structural information. Tools to mitigate, understand and even use this result have been developed over many decades and have been extended to the solution techniques that have been used here. The dose used for structural studies with X-rays is often measured in the kilogray to megagray range. In the therapeutic setting or radiation environments that impact health, doses are measured in grays or less, with X-ray doses of above 100–200 mGy being known to cause adverse health effects. A dose of 100 mGy is the equivalent of about 1000 conventional chest X-rays, 0.1–2.0 Gy, and, as described above, single doses of 2–30 Gy are used for moderate and high-dose radiotherapy (Vaiserman *et al.*, 2018; Timmerman *et al.*, 2010; Gao *et al.*, 2019; Lo *et al.*, 2010). While there are differences in X-ray sources and energy levels, to a first approximation the study here has been conducted close to the doses that are experienced at therapeutic levels. There are a wealth of biological macromolecules that are known or thought to be impacted by low-dose radiation.

The experiments described were challenging, with the maximum total dose used being hundreds of grays. This limited the analysis techniques owing to the low signal and high noise. However, it may be possible to use high dose and short exposure to outrun some of the damage linked to health effects (Owen *et al.*, 2012) or to use X-ray free-electron laser sources, where the pulse duration can limit any damage seen in the electron-density maps to primary effects only (Chapman *et al.*, 2014). The same tools and discoveries that have impacted radiation damage at crystallographic doses (kilograys to megagrays) can be extended to the study of biology at doses at

the lower end of the spectrum to provide meaningful improvement of the knowledge surrounding therapeutic uses of radiation. This represents a shift in the radiation-damage field in structural biology where, rather than mitigate damage, the damage itself is studied to understand biologically relevant mechanisms.

5. Related literature

The following references are cited in the supporting information for this article: Dyer *et al.* (2014), Gasteiger *et al.* (2007) and Yang *et al.* (2012).

Acknowledgements

The furin-bio-his and TGFβ1-bio-his plasmids were generously provided by Dr Gavin Wright (Addgene plasmids #51755 and #52185). We are grateful to Dr Andrei Bakin (RPCCC, Buffalo, New York, USA) for providing the NMuMG cells. Dr James Holton is thanked for useful discussions and Dr Ivo Tews for his input. The authors thank the Pharmaceutical Sciences Instrumentation facility, University at Buffalo, State University of New York for the use of the CD instrument, which was obtained by Shared Instrumentation Grant S10-RR013665 from the National Center for Research Resources, National Institute of Health. The SAXS work was conducted at the Advanced Light Source (ALS), a national user facility operated by Lawrence Berkeley National Laboratory on behalf of the Department of Energy, Office of Basic Energy Sciences through the Integrated Diffraction Analysis Technologies (IDAT) program supported by the DOE Office of Biological and Environmental Research. Additional support comes from National Institutes of Health project ALS-ENABLE (P30 GM124169) and High-End Instrumentation Grant S10OD018483. All relevant SAXS data are available in the supporting information. The experimental SAXS data have been deposited in SASBDB (the Small Angle Scattering Biological Data Bank; Valentini *et al.*, 2015) under codes SASDFD2 and SASDFE2.

Funding information

This work was supported by a grant from the National Science Foundation (1231306) awarded to EHS.

References

Allan, E. G., Kander, M. C., Carmichael, I. & Garman, E. F. (2013). *J. Synchrotron Rad.* **20**, 23–36.
Annes, J. P., Munger, J. S. & Rifkin, D. B. (2003). *J. Cell Sci.* **116**, 217–224.
Arany, P. R., Cho, A., Hunt, T. D., Sidhu, G., Shin, K., Hahm, E., Huang, G. X., Weaver, J., Chen, A. C.-H., Padwa, B. L., Hamblin, M. R., Barcellos-Hoff, M. H., Kulkarni, A. B. & Mooney, D. J. (2014). *Sci. Transl. Med.* **6**, 238ra69.
Barcellos-Hoff, M. H. (1993). *Cancer Res.* **53**, 3880–3886.
Barcellos-Hoff, M. H., Derynck, R., Tsang, M. L.-S. & Weatherbee, J. A. (1994). *J. Clin. Invest.* **93**, 892–899.
Barcellos-Hoff, M. H. & Dix, T. A. (1996). *Mol. Endocrinol.* **10**, 1077–1083.
Barnes, J., Warejcka, D., Simpliciano, J., Twining, S. & Steet, R. (2012). *J. Biol. Chem.* **287**, 7526–7534.
Bernadó, P., Mylonas, E., Petoukhov, M. V., Blackledge, M. & Svergun, D. I. (2007). *J. Am. Chem. Soc.* **129**, 5656–5664.
Bierie, B. & Moses, H. L. (2006). *Nature Rev. Cancer*, **6**, 506–520.
Brooks-Bartlett, J. C., Batters, R. A., Bury, C. S., Lowe, E. D., Ginn, H. M., Round, A. & Garman, E. F. (2017). *J. Synchrotron Rad.* **24**, 63–72.
Brunner, A. M., Marquardt, H., Malacko, A. R., Lioubin, M. N. & Purchio, A. F. (1989). *J. Biol. Chem.* **264**, 13660–13664.
Buscemi, L., Ramonet, D., Klingberg, F., Formey, A., Smith-Clerc, J., Meister, J. J. & Hinz, B. (2011). *Curr. Biol.* **21**, 2046–2054.
Cecarini, V., Gee, J., Fioretti, E., Amici, M., Angeletti, M., Eleuteri, A. M. & Keller, J. N. (2007). *Biochim. Biophys. Acta*, **1773**, 93–104.
Chapman, H. N., Caleman, C. & Timneanu, N. (2014). *Philos. Trans. R. Soc. Lond. B Biol. Sci.* **369**, 20130313.
Dong, X., Zhao, B., Iacob, R. E., Zhu, J., Koksal, A. C., Lu, C., Engen, J. R. & Springer, T. A. (2017). *Nature (London)*, **542**, 55–59.
Drumm, M. L., Konstan, M. W., Schluchter, M. D., Handler, A., Pace, R., Zou, F., Zariwala, M., Fargo, D., Xu, A., Dunn, J. M., Darrah, R. J., Dorfman, R., Sandford, A. J., Corey, M., Zielenski, J., Durie, P., Goddard, K., Yankaskas, J. R., Wright, F. A. & Knowles, M. R. (2005). *N. Engl. J. Med.* **353**, 1443–1453.
Dyer, K. N., Hammel, M., Rambo, R. P., Tsutakawa, S. E., Rodic, I., Classen, S., Tainer, J. A. & Hura, G. L. (2014). *Methods Mol. Biol.* **1091**, 245–258.
Ehrhart, E. J., Segarini, P., Tsang, M. L., Carroll, A. G. & Barcellos-Hoff, M. H. (1997). *FASEB J.* **11**, 991–1002.
Franke, D., Jeffries, C. M. & Svergun, D. I. (2015). *Nature Methods*, **12**, 419–422.
Franke, D., Petoukhov, M. V., Konarev, P. V., Panjkovich, A., Tuukkanen, A., Mertens, H. D. T., Kikhney, A. G., Hajizadeh, N. R., Franklin, J. M., Jeffries, C. M. & Svergun, D. I. (2017). *J. Appl. Cryst.* **50**, 1212–1225.
Gabriely, G., da Cunha, A. P., Rezende, R. M., Kenyon, B., Madi, A., Vandeventer, T., Skillin, N., Rubino, S., Garo, L., Mazzola, M. A., Kolypetri, P., Lanser, A. J., Moreira, T., Faria, A. M. C., Lassmann, H., Kuchroo, V., Murugaiyan, G. & Weiner, H. L. (2017). *Sci. Immunol.* **2**, eaaj1738.
Gao, R. W., Olivier, K. R., Park, S. S., Davis, B. J., Pisansky, T. M., Choo, R., Kwon, E. D., Karnes, R. J., Harmsen, W. S. & Stish, B. J. (2019). *Adv. Radiat. Oncol.* **4**, 314–322.
Garman, E. & Owen, R. L. (2007). *Methods Mol. Biol.* **364**, 1–18.
Garman, E. F. & Weik, M. (2017). *Methods Mol. Biol.* **1607**, 467–489.
Gasteiger, E., Hoogland, C., Gattiker, A., Duvaud, S., Wilkins, M. R., Appel, R. D. & Bairoch, A. (2005). *The Proteomics Protocols Handbook*, edited by J. M. Walker, pp. 571–607. Totowa: Humana Press.
Grune, T., Reinheckel, T. & Davies, K. J. (1997). *FASEB J.* **11**, 526–534.
Hochanadel, C. J. (1952). *J. Phys. Chem.* **56**, 587–594.
Hopkins, J. B. & Thorne, R. E. (2016). *J. Appl. Cryst.* **49**, 880–890.
ICRP (2007). *Ann. ICRP*, **37**, 1–332.
Jeffries, C. M., Graewert, M. A., Svergun, D. I. & Blanchet, C. E. (2015). *J. Synchrotron Rad.* **22**, 273–279.
Jobling, M. F., Mott, J. D., Finnegan, M. T., Jurukovski, V., Erickson, A. C., Walian, P. J., Taylor, S. E., Ledbetter, S., Lawrence, C. M., Rifkin, D. B. & Barcellos-Hoff, M. H. (2006). *Radiat. Res.* **166**, 839–848.
Kinoshita, A., Saito, T., Tomita, H., Makita, Y., Yoshida, K., Ghadami, M., Yamada, K., Kondo, S., Ikegawa, S., Nishimura, G., Fukushima, Y., Nakagomi, T., Saito, H., Sugimoto, T., Kamegaya, M., Hisa, K., Murray, J. C., Taniguchi, N., Niikawa, N. & Yoshiura, K. (2000). *Nature Genet.* **26**, 19–20.
Kohn, H. I. & Kallman, R. F. (1957). *Radiat. Res.* **6**, 137–147.
Kuwamoto, S., Akiyama, S. & Fujisawa, T. (2004). *J. Synchrotron Rad.* **11**, 462–468.

Lawrence, D. A., Pircher, R. & Jullien, P. (1985). *Biochem. Biophys. Res. Commun.* **133**, 1026–1034.
Lo, S. S., Fakiris, A. J., Chang, E. L., Mayr, N. A., Wang, J. Z., Papiez, L., Teh, B. S., McGarry, R. C., Cardenes, H. R. & Timmerman, R. D. (2010). *Nature Rev. Clin. Oncol.* **7**, 44–54.
Lyons, R. M., Keski-Oja, J. & Moses, H. L. (1988). *J. Cell Biol.* **106**, 1659–1665.
Mavridis, L. & Janes, R. W. (2017). *Bioinformatics*, **33**, 56–63.
McMahon, G. A., Dignam, J. D. & Gentry, L. E. (1996). *Biochem. J.* **313**, 343–351.
Meents, A., Gutmann, S., Wagner, A. & Schulze-Briese, C. (2010). *Proc. Natl Acad. Sci. USA*, **107**, 1094–1099.
Micsonai, A., Wien, F., Bulyáki, E., Kun, J., Moussong, E., Lee, Y.-H., Goto, Y., Réfrégiers, M. & Kardos, J. (2018). *Nucleic Acids Res.* **46**, W315–W322.
Munger, J. S., Huang, X., Kawakatsu, H., Griffiths, M. J., Dalton, S. L., Wu, J., Pittet, J. F., Kaminski, N., Garat, C., Matthay, M. A., Rifkin, D. B. & Sheppard, D. (1999). *Cell*, **96**, 319–328.
Owen, R. L., Axford, D., Nettleship, J. E., Owens, R. J., Robinson, J. I., Morgan, A. W., Doré, A. S., Lebon, G., Tate, C. G., Fry, E. E., Ren, J., Stuart, D. I. & Evans, G. (2012). *Acta Cryst.* D**68**, 810–818.
Owen, R. L., Rudiño-Piñera, E. & Garman, E. F. (2006). *Proc. Natl Acad. Sci. USA*, **103**, 4912–4917.
Paithankar, K. S., Owen, R. L. & Garman, E. F. (2009). *J. Synchrotron Rad.* **16**, 152–162.
Sato, Y. & Rifkin, D. B. (1989). *J. Cell Biol.* **109**, 309–315.
Semisotnov, G. V., Kihara, H., Kotova, N. V., Kimura, K., Amemiya, Y., Wakabayashi, K., Serdyuk, I. N., Timchenko, A. A., Chiba, K., Nikaido, K., Ikura, T. & Kuwajima, K. (1996). *J. Mol. Biol.* **262**, 559–574.
Shi, M., Zhu, J., Wang, R., Chen, X., Mi, L., Walz, T. & Springer, T. A. (2011). *Nature (London)*, **474**, 343–349.
Squier, T. C. (2001). *Exp. Gerontol.* **36**, 1539–1550.
Sun, Y., Vandenbriele, C., Kauskot, A., Verhamme, P., Hoylaerts, M. F. & Wright, G. J. (2015). *Mol. Cell. Proteomics*, **14**, 1265–1274.
Sutton, K. A., Black, P. J., Mercer, K. R., Garman, E. F., Owen, R. L., Snell, E. H. & Bernhard, W. A. (2013). *Acta Cryst.* D**69**, 2381–2394.
Svergun, D. I., Koch, M. H. J., Timmins, P. & May, R. P. (2013). *Small Angle X-ray and Neutron Scattering from Solutions of Biological Macromolecules.* Oxford University Press.
Timmerman, R., Paulus, R., Galvin, J., Michalski, J., Straube, W., Bradley, J., Fakiris, A., Bezjak, A., Videtic, G., Johnstone, D., Fowler, J., Gore, E. & Choy, H. (2010). *JAMA*, **303**, 1070–1076.
Trewhella, J., Duff, A. P., Durand, D., Gabel, F., Guss, J. M., Hendrickson, W. A., Hura, G. L., Jacques, D. A., Kirby, N. M., Kwan, A. H., Pérez, J., Pollack, L., Ryan, T. M., Sali, A., Schneidman-Duhovny, D., Schwede, T., Svergun, D. I., Sugiyama, M., Tainer, J. A., Vachette, P., Westbrook, J. & Whitten, A. E. (2017). *Acta Cryst.* D**73**, 710–728.
Tria, G., Mertens, H. D. T., Kachala, M. & Svergun, D. I. (2015). *IUCrJ*, **2**, 207–217.
Vaiserman, A., Koliada, A., Zabuga, O. & Socol, Y. (2018). *Dose Response*, **16**, 1559325818796331.
Valentini, E., Kikhney, A. G., Previtali, G., Jeffries, C. M. & Svergun, D. I. (2015). *Nucleic Acids Res.* **43**, D357–D363.
Webb, B. & Sali, A. (2014). *Methods Mol. Biol.* **1137**, 1–15.
Weik, M., Ravelli, R. B. G., Kryger, G., McSweeney, S., Raves, M. L., Harel, M., Gros, P., Silman, I., Kroon, J. & Sussman, J. L. (2000). *Proc. Natl Acad. Sci. USA*, **97**, 623–628.
Wilkinson, K. A., Martin, T. D., Reba, S. M., Aung, H., Redline, R. W., Boom, W. H., Toossi, Z. & Fulton, S. A. (2000). *Infect. Immun.* **68**, 6505–6508.
Winklmair, D. (1971). *Arch. Biochem. Biophys.* **147**, 509–514.
Yang, Z., Lasker, K., Schneidman-Duhovny, D., Webb, B., Huang, C. C., Pettersen, E. F., Goddard, T. D., Meng, E. C., Sali, A. & Ferrin, T. E. (2012). *J. Struct. Biol.* **179**, 269–278.
Zhao, B., Xu, S., Dong, X., Lu, C. & Springer, T. A. (2018). *J. Biol. Chem.* **293**, 1579–1589.
Zou, Z. & Sun, P. D. (2004). *Protein Expr. Purif.* **37**, 265–272.